






Magnetic field effects on the valence band of AlGaAs and InGaAsP parabolic quantum wellsM. A. Tito Patricio ^{1,2} L. Villegas-Lelovsky ^{3,4} E. R. Cardozo de Oliveira ⁴ G. E. Marques,⁴
R. R. LaPierre ⁵ A. I. Toropov,⁶ and Yu. A. Pusep ^{1,*}¹*São Carlos Institute of Physics, University of São Paulo, P.O. Box 369, 13560-970 São Carlos, São Paulo, Brazil*²*Facultad de Ciencias Físicas, Universidad Nacional Mayor de San Marcos, P.O.-Box 14-0149 Lima 14, Peru*³*Departamento de Física, IGCE, Universidade Estadual Paulista, 13506-900 Rio Claro, São Paulo, Brazil*⁴*Departamento de Física, Universidade Federal de São Carlos, 13565-905 São Carlos, São Paulo, Brazil*⁵*Centre for Emerging Device Technologies, Department of Engineering Physics, McMaster University, Hamilton, Ontario L8S 4L7, Canada*⁶*Institute of Semiconductor Physics, 630090 Novosibirsk, Russia*

(Received 1 July 2022; revised 16 June 2023; accepted 30 June 2023; published 21 July 2023)

The influence of the valence band structure on the optical properties of quantum wells with a parabolic potential, consisting of $\text{Al}_x\text{Ga}_{1-x}\text{As}$ and $\text{In}_{1-x}\text{Ga}_x\text{As}_y\text{P}_{1-y}$ alloys, is studied and compared. The distribution of photogenerated carriers over the parabolic potential is found to be responsible for specific selection rules: the recombination due to only odd-indexed confined levels is observed. The reason for this is the accumulation of photogenerated holes at the center of the parabolic potential, which results in interband electron-hole recombination occurring at the center of the parabolic quantum wells. Furthermore, a specific valence band structure is found to be responsible for the magnetic-field-induced change in the photoluminescence circular polarization. In particular, at a certain magnetic field, the hybridization of the states of a heavy hole and a light hole results in the intersection of Landau levels with different spins, which leads to the observed change in the circular polarization of photoluminescence. The processes of long-term spin relaxation of heavy holes in both studied parabolic quantum wells are demonstrated, and the corresponding times are obtained.

DOI: [10.1103/PhysRevB.108.035416](https://doi.org/10.1103/PhysRevB.108.035416)**I. INTRODUCTION**

Wide semiconductor parabolic quantum wells (PQWs) have been suggested and realized as structures where a high mobility of quasi-three-dimensional confined electrons can be achieved due to a remote doping [1,2]. Later, several specific properties of the parabolic potential important in device applications were found. Under an applied electric field, PQWs reveal optical rectification (when a light sinusoidal electric field turns into a DC polarization) [3]. Electrically and optically pumped coherent THz emission has been observed in PQWs [4,5]. Such a nonlinear optical performance of PQWs has the potential for device applications in laser amplifiers, photodetectors, high-speed electro-optical modulators, etc. [6,7]. Moreover, an efficient electrical spin manipulation can be achieved in PQWs subject to the magnetic field and electric bias through the relativistic mechanisms of spin-orbit coupling [8–11]. Such a spin-orbit interaction tuning is one of the key ingredients for spintronic devices. As a consequence of the generalized Kohn's theorem [12], the excitation energy spectrum of the ideal PQW is independent of the electron-electron interaction and therefore, it is very robust against variation of the number of electrons [13] and any external perturbations that change the electron concentration. This results in stability of electronic devices based on PQWs. Until now, all the reported realizations of the PQW potential profile were

based on $\text{Al}_x\text{Ga}_{1-x}\text{As}$ alloy, except for the $\text{Al}_x\text{Ga}_y\text{In}_{1-x-y}\text{As}$ and Ge/SiGe PQWs reported in Refs. [14] and [15], respectively.

The effect of electron screening on the potentials of the conduction and valence bands in a wide PQW is shown in Fig. 1. In the insulating case, the energy levels confined to the conduction and valence band of the PQWs form uniformly spaced levels which reflect harmonic oscillator-like electron and hole levels. In a metallic PQW, electrons from donors located in barriers enter the PQW and screen the parabolic potential of the conduction band, forming a square quantum well with the corresponding quantized levels, while the parabolicity of the potential in the valence band becomes even stronger. To date, most of the related works were focused on investigation of the electron properties of PQWs. However, given the optical response in the most commonly used n-doped PQWs [4,5,7,10,16,17], the electrons in the conduction band are inert with respect to optical properties. In this case, the energy structure of the valence band becomes of great importance. Information about the valence band structure and its effect on the optical polarization is central for spin manipulation in spintronic devices based on PQWs, especially those using spin injection by holes [18,19]. In such n-doped PQWs the circular polarization of the optical emission is determined by processes of spin hole relaxation. Information about the processes of spin relaxation in the valence band of the PQW can be obtained using measurements of circularly polarized photoluminescence (PL). To the best of our knowledge, no such data have been published so far. In this paper, we report

*pusep@ifsc.usp.br

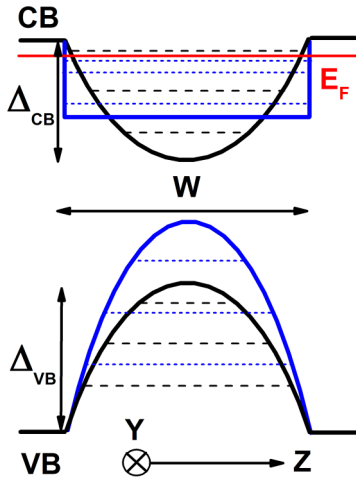


FIG. 1. Schematic of insulating (black lines) and metallic (blue lines, with Fermi level in red) PQWs of width W with corresponding quantized levels. Δ_{CB} and Δ_{VB} are conduction and valence band quantum well depths related to the insulating case, respectively. Directions Y and Z used in Sec. IV are shown.

on the study of the valence band structure and its impact on polarization properties of the PQW based on $\text{Al}_x\text{Ga}_{1-x}\text{As}$ ternary and $\text{In}_{1-x}\text{Ga}_x\text{As}_y\text{P}_{1-y}$ quaternary alloys. In addition, the processes of spin relaxation of holes are studied.

The article is organized as follows: details of the experiment, including a description of the structure of the samples, a presentation of the technical setup, and an explanation of the observed optical processes, are given in the next Sec. II. The calculated energy structure of the samples under study and their optical and magneto-optical characteristics are given in Sec. III. The analysis of the obtained results together with time-resolved PL data is presented in Sec. IV, and the conclusions are summarized in Sec. V.

II. EXPERIMENTAL DETAILS

The samples studied here were selectively doped 240 nm thick $\text{Al}_x\text{Ga}_{1-x}\text{As}$ and 70 nm thick $\text{In}_{1-x}\text{Ga}_x\text{As}_y\text{P}_{1-y}$ PQWs, both grown on (100) semi-insulating GaAs substrates. The PQWs were sandwiched by short-period GaAs/AIAs superlattice doping structures containing Si delta-doped layers. Two δ -doped Si layers were placed on both sides of the PQW in the superlattice barriers leaving undoped 12.4-nm-thick spacers separating the PQW and dopant Si atoms. An additional δ -doped Si layer was inserted between the doping δ layer and the sample surface in order to screen the surface charge. The $\text{Al}_x\text{Ga}_{1-x}\text{As}$ PQW was grown by molecular beam epitaxy with a 45-nm $\text{Al}_{0.36}\text{Ga}_{0.64}\text{As}$ buffer layer. The composition x of the $\text{Al}_x\text{Ga}_{1-x}\text{As}$ PQW was continuously changed from 0.24 to 0 and then to 0.24 in order to achieve a gradual parabolic potential profile with Ga and Al fluxes controlled by individual temperatures of the effusion cell, at a constant As pressure. The densities of the doping and the additional screening δ Si layers were 1.8×10^{12} and $2.0 \times 10^{12} \text{ cm}^{-2}$, respectively. The $\text{In}_{1-x}\text{Ga}_x\text{As}_y\text{P}_{1-y}$ PQW was grown by gas source molecular beam epitaxy with a 50-nm GaAs layer followed by a 45-nm $\text{Al}_{0.36}\text{Ga}_{0.64}\text{As}$ buffer layer. In this case the PQW bandgap varied parabolically from 1.9 eV

($\text{In}_{0.49}\text{Ga}_{0.51}\text{P}$ layer) down to 1.42 eV (GaAs layer) and then returned to 1.9 eV ($\text{In}_{0.49}\text{Ga}_{0.51}\text{P}$) in digital steps comprised of 49 layers, each 1.43 nm thick. During the growth In, Ga, and Al compositions were controlled by separate effusion cell temperatures, while As and P compositions were set by the mass flow control of AsH_3 and PH_3 precursors to a gas cracker (producing As_2 and P_2), while maintaining a lattice match to GaAs. The density of the doping and the additional screening δ Si layers were 2.2×10^{12} and $2.5 \times 10^{12} \text{ cm}^{-2}$, respectively. The centers of both PQWs are mostly formed by GaAs, whereas the sides are different, composed of either $\text{Al}_x\text{Ga}_{1-x}\text{As}$ or $\text{In}_{1-x}\text{Ga}_x\text{As}_y\text{P}_{1-y}$ alloys.

PL measurements were carried out at the temperature 1.6 K in the range of the magnetic field 0 -10 T applied perpendicular to the surface plane. The samples were excited by a diode laser (Pico Quant - LDH-730) emitting at 470 nm in a continuous mode. The PL was collected by an Ocean Optics Inc. HR4000 high-resolution spectrometer. In order to measure the time-resolved PL, the samples were pumped by the same diode laser emitting at 730 nm, which generated 70 ps pulses at the frequency 80 MHz. The signal was dispersed by a SPEX 500M spectrometer. The PL transients were detected by a PicoQuant Hybrid PMT detector. Separation between the right (σ^+) and left (σ^-) circularly polarized components was achieved using a quarter-wave plate and a linear polarizer setup placed in front of the sample.

The analysis of the symmetry of optical transitions based on the general group theory shows that in zinc-blende crystals, optical transitions occur at the point Γ predominantly between the Γ_{15} states of the valence band and the Γ_1 states of the conduction band [20]. The optical selection rules are based on the conservation of energy, momentum and angular momentum. Consideration of the angular momentum is fundamental in the case of circularly polarized absorption and emission. When a circularly polarized photon is absorbed, its angular momentum is distributed between the photoexcited electron and hole according to the selection rules determined by the band structure of the semiconductor. In the PQWs studied, the circularly polarized PL spectrum originates from the recombination between the electrons ($J_e = 1/2$, $j_{ez} = \pm 1/2$), heavy holes (hh) ($J_h = 3/2$, $j_{hz} = \pm 3/2$), and light holes (lh) ($J_h = 3/2$, $j_{hz} = \pm 1/2$), where $J_{e(h)}$ and $j_{e(h)z}$ denote the electron (hole) band-edge Bloch angular momentum and its z component, respectively.

The PL circular polarization was changed by inverting the direction of the magnetic field. The circular polarization of PL emitted from confined levels can be determined by the usual formula:

$$P_\sigma = \frac{I^- - I^+}{I^- + I^+}, \quad (1)$$

where I^+ and I^- are the integrated PL intensities related to confined levels measured in σ^+ and σ^- polarizations, respectively.

III. SAMPLE CHARACTERIZATION

The potential energy profiles around the $\text{Al}_x\text{Ga}_{1-x}\text{As}$ and $\text{In}_{1-x}\text{Ga}_x\text{As}_y\text{P}_{1-y}$ PQWs (without additional δ -doped Si layer) are shown in Figs. 2(a) and 2(b). The electron and the heavy

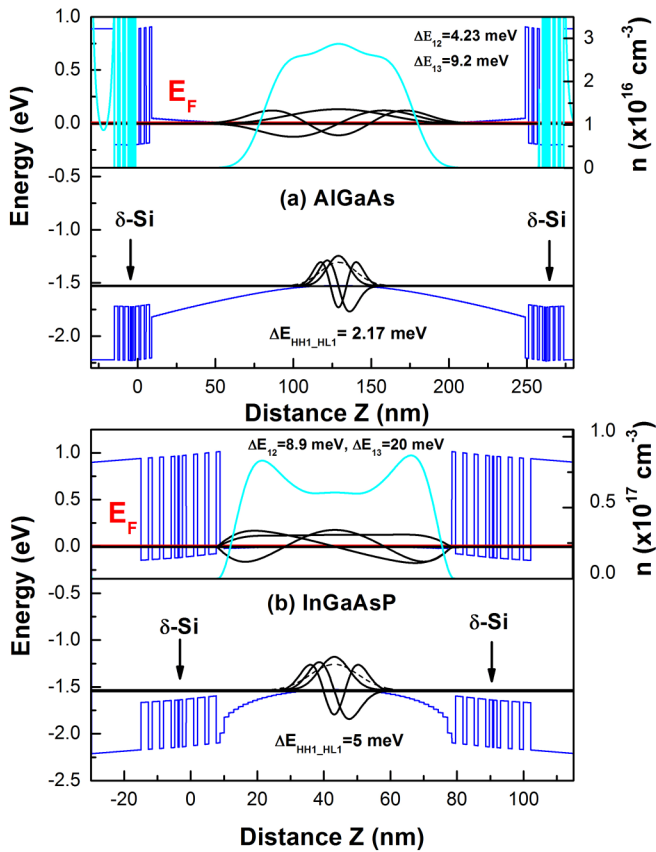


FIG. 2. The calculated $\text{Al}_x\text{Ga}_{1-x}\text{As}$ (a) and $\text{In}_{1-x}\text{Ga}_x\text{As}_y\text{P}_{1-y}$ (b) PQW band energy structures and the wave functions of the three relevant lowest confined levels of the conduction and heavy hole valence bands (black lines). The wave functions of the lowest energy light hole confined levels are shown by black dashed lines. The energy gaps between the relevant levels are shown on the respective panels. The distribution of the electron density in the conduction bands is shown by cyan lines. Blue and red lines show the energy potential profile of the structures under investigation and the position of the Fermi level, respectively.

hole wave functions of three relevant confined energy levels below the Fermi level are shown. The charge density and the potential are calculated self-consistently using a one-electron one-dimensional Schrödinger-Poisson equation solver [21]. In the course of calculations, the discretized parabolic potentials were constructed from a sequence of corresponding alloy layers with a thickness of 2 nm and 1.43 nm each for $\text{Al}_x\text{Ga}_{1-x}\text{As}$ and $\text{In}_{1-x}\text{Ga}_x\text{As}_y\text{P}_{1-y}$ PQWs, respectively. At each layer boundary the effective mass discontinuity was determined according to the finite difference method, while the eigenvalues and eigenfunctions close to the bottom of the PQW potential profile were calculated numerically from the discrete Schrödinger equation. In both PQWs, the electrostatic repulsion among electrons results in a nearly square conduction band potential profile. As a consequence, the electrons are confined to the effective square potential. In the $\text{Al}_x\text{Ga}_{1-x}\text{As}$ PQW, an approximately uniform electron distribution is located in the central region of about 100 nm, while in the $\text{In}_{1-x}\text{Ga}_x\text{As}_y\text{P}_{1-y}$ PQW electrons are almost uniformly distributed over the entire width of the PQW. At the same

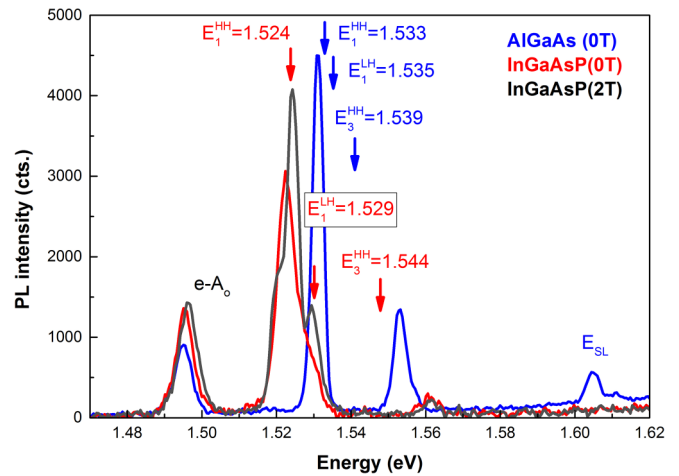


FIG. 3. Unpolarized PL spectra measured for the $\text{Al}_x\text{Ga}_{1-x}\text{As}$ (red line) and $\text{In}_{1-x}\text{Ga}_x\text{As}_y\text{P}_{1-y}$ (blue line) PQWs at the temperature 1.6 K in zero magnetic field. A black line is the PL spectrum of the $\text{In}_{1-x}\text{Ga}_x\text{As}_y\text{P}_{1-y}$ PQW measured in the magnetic field 2 T. The arrows indicate the calculated recombination energies related to the corresponding confined levels. The peak $e\text{-A}_0$ relates due to the recombination of the conduction band electrons with the holes bound on neutral carbon acceptors.

time, the valence band potential remains parabolic, which leads to the fact that holes are located predominantly in the center of the PQW. As will be shown below, such different distribution of the electron and hole densities drastically affects the recombination determined by selection rules. The corresponding electron density distribution, built up from a superposition of wave functions for three populated confining levels below the Fermi level, is shown in Figs. 2(a) and 2(b) by cyan lines. The calculations show the comparable effective widths of both PQWs (about 100 and 70 nm for the $\text{Al}_x\text{Ga}_{1-x}\text{As}$ and the $\text{In}_{1-x}\text{Ga}_x\text{As}_y\text{P}_{1-y}$ PQWs, respectively) established by the spatial distribution of the electron density along the growth direction.

Unpolarized PL spectra of both PQWs studied here measured in zero magnetic field are depicted in Fig. 3. Each PQW emits three distinct PL lines. The low energy line at 1.495 eV ($e\text{-A}_0$) is due to the recombination of the conduction band electrons with the holes bound on neutral carbon acceptors (free to bound transition) [22]. The most intense PL lines E_1^{HH} are caused by the recombination of the electrons and photogenerated heavy holes confined to the lowest energy levels e_1 and hh_1 , respectively. According to the calculation, in both PQWs the PL line E_1^{LH} due to the lowest energy light hole confined levels lh_1 is found in close proximity to the E_1^{HH} energy. Therefore the recombination of light holes is spectroscopically indistinguishable in the $\text{Al}_x\text{Ga}_{1-x}\text{As}$ PQW, while it appears to be a shoulder, or a weak peak for $\text{In}_{1-x}\text{Ga}_x\text{As}_y\text{P}_{1-y}$ PQW for zero and 2-T magnetic field, respectively. A slightly larger gap between the hh_1 and lh_1 confined levels found in the $\text{In}_{1-x}\text{Ga}_x\text{As}_y\text{P}_{1-y}$ PQW (5 meV versus 2.2 meV in the $\text{Al}_x\text{Ga}_{1-x}\text{As}$ PQW) results in their separation when the magnetic field is applied. In both the PQWs the calculated energy E_3^{HH} of the recombination between the e_3 and hh_3 levels is lower than the observed third PL peak position. Several reasons may cause larger energy gap between the

TABLE I. Experimentally determined and calculated energies of optical transitions observed in the PL spectra of AlGaAs and InGaAsP PQWs.

| Transition | AlGaAs | | InGaAsP | |
|-------------------|-----------|-----------|-----------|-----------|
| | Expt., eV | Calc., eV | Expt., eV | Calc., eV |
| E_1^{HH} | 1.531 | 1.533 | 1.524 | 1.524 |
| E_1^{LH} | - | 1.535 | 1.529 | 1.529 |
| E_3^{HH} | 1.553 | 1.539 | 1.560 | 1.544 |

observed E_1^{HH} and E_3^{HH} PL peak positions. Among them are the effect of exchange interaction on the gap between quantum well subbands [23] and different excitonic binding energies for different pairs of conduction and valence band confined levels [24], which were not considered in the band structure calculations. For clarity, the photoluminescence peak positions observed in the $\text{Al}_x\text{Ga}_{1-x}\text{As}$ and the $\text{In}_{1-x}\text{Ga}_x\text{As}_y\text{P}_{1-y}$ PQWs, together with the corresponding calculated values, are given in Table I. The observed PL spectra reveal no lines which may be assigned to the recombination between the even confined levels e2 and hh2. An absence of the detectable emission from the even-indexed confined levels is a consequence of different confining regions for electrons and holes. As shown in Fig. 2, the holes are confined to a much narrower region in the center of a PQW where the density of even confined electrons vanishes. Therefore the probability of the recombination between the spatially separated even confined levels of an electron and a hole is small as compared to the odd levels. Such a character of the recombination reduces a number of recombination channels in PQWs and makes emissions from the odd confined levels stronger.

Furthermore, as follows from the results of calculations presented in Fig. 2, a significant number of electrons

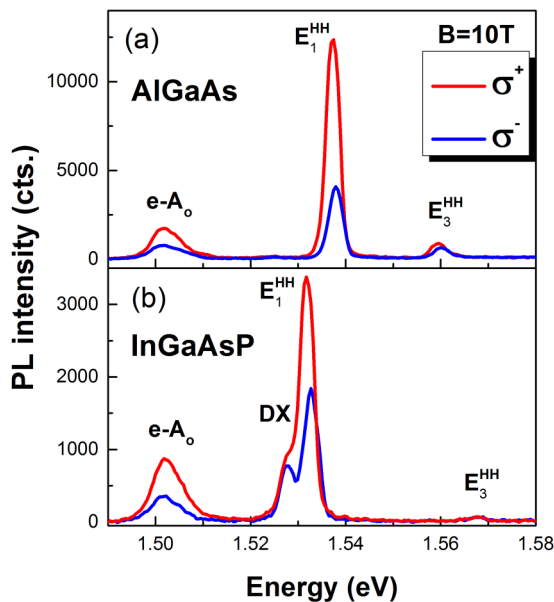


FIG. 4. PL spectra measured with different circular polarizations in the magnetic field 10 T in the $\text{Al}_x\text{Ga}_{1-x}\text{As}$ (a) and $\text{In}_{1-x}\text{Ga}_x\text{As}_y\text{P}_{1-y}$ (b) PQWs at the temperature 1.6 K.

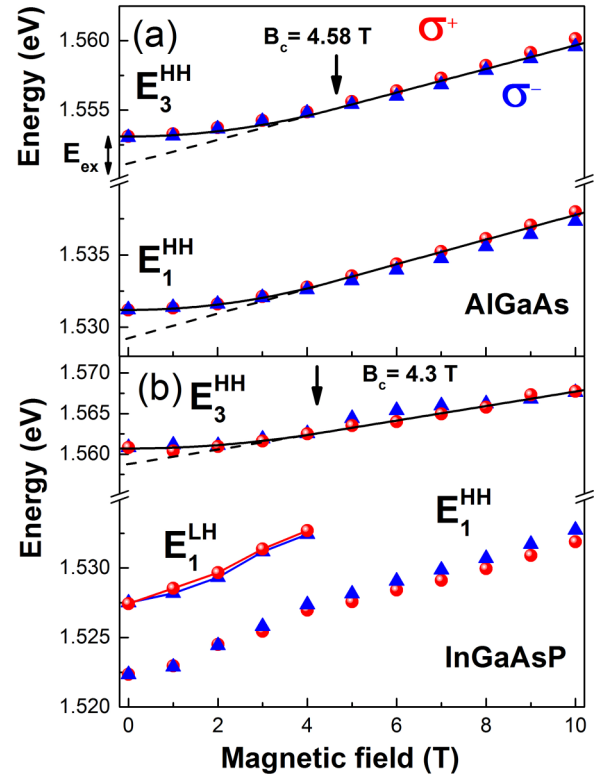


FIG. 5. The energies of the differently polarized PL lines (red - σ^+ , blue - σ^-) corresponding to the levels confined to the $\text{Al}_x\text{Ga}_{1-x}\text{As}$ (a) and $\text{In}_{1-x}\text{Ga}_x\text{As}_y\text{P}_{1-y}$ (b) PQWs, measured as a function of the magnetic field at $T = 1.6$ K. Solid lines were calculated according to Eqs. (2) and (3) with the reduced exciton effective masses $0.068m_0$ (a) and $0.064m_0$ (b), respectively. Dashed lines are high magnetic field extrapolations according to Eq. (3).

reside in the barrier GaAs/AlAs short-period superlattice in the $\text{Al}_x\text{Ga}_{1-x}\text{As}$ PQW, while no electrons were found in the barrier superlattice in the $\text{In}_{1-x}\text{Ga}_x\text{As}_y\text{P}_{1-y}$ PQW. Accordingly, a weak PL line observed in the $\text{Al}_x\text{Ga}_{1-x}\text{As}$ PQW around 1.6 eV emerges from recombination in the barrier GaAs/AlAs superlattice, while no such emission was detected in the $\text{In}_{1-x}\text{Ga}_x\text{As}_y\text{P}_{1-y}$ PQW.

The PL spectra measured in both studied PQWs with different circular polarizations are shown in Fig. 4. These data demonstrate a significant magnetic-field-induced polarization of the observed optical transitions, which will be analyzed and discussed below in Sec. IV. It is worth noting that the application of a magnetic field to the $\text{In}_{1-x}\text{Ga}_x\text{As}_y\text{P}_{1-y}$ PQW reveals a new PL line approximately 5 meV below the E_1^{HH} line, which may belong to DX centers (exciton bound to neutral donor). The energies of all the PL lines measured with different circular polarizations in the PQWs studied here are shown in Figs. 5(a) and 5(b) as a function of the magnetic field. The exciton diamagnetic shift causes nonlinear dependence of the observed PL energies as a function of the magnetic field [25] according to the following expressions [26]:

$$E(B) = E_0 + \frac{E_{\text{ex}}}{B_c^2} B^2, \quad \text{for } B < B_c = \frac{2\hbar}{ea_B^2}, \quad (2)$$

$$E(B) = E_0 - E_{\text{ex}} + \frac{2E_{\text{ex}}}{B_c} B, \quad \text{for } B > B_c, \quad (3)$$

where E_0 is the transition energy without magnetic field, the exciton binding energy $E_{\text{ex}} = \hbar^2/2\mu_{\text{ex}}a_B^2$, a_B is the effective Bohr radius, and μ_{ex} is the reduced exciton mass. Thus, fitting the transition energies measured as a function of the magnetic field makes it possible to determine the exciton binding energy.

Clear diamagnetic shifts are observed for the E_1^{HH} and E_3^{HH} transitions in the $\text{Al}_x\text{Ga}_{1-x}\text{As}$ PQW and for the E_3^{HH} transition in the $\text{In}_{1-x}\text{Ga}_x\text{As}_y\text{P}_{1-y}$ PQW. The uncertainty in determining the energy of the E_1^{HH} transition in the $\text{In}_{1-x}\text{Ga}_x\text{As}_y\text{P}_{1-y}$ PQW, caused by the close location of the E_1^{LH} transition, does not allow one to observe the corresponding diamagnetic shift. Moreover, in this PQW the recombination E_1^{LH} vanishes already in the magnetic field above 4 T due to depopulation of the related light hole confined level. Therefore the exciton binding energy in the $\text{In}_{1-x}\text{Ga}_x\text{As}_y\text{P}_{1-y}$ PQW was determined using the PL peak positions of the E_3^{HH} transition. The results of the best fits are shown in Fig. 5. The resulting exciton binding energies are about 2 meV in both PQWs studied. This value is much lower than the exciton binding energies of about 10–15 meV expected in both PQWs [27,28]. The lower binding energies of excitons obtained in the PQW studied here are due to the screening of the electron-hole Coulomb interaction by free electrons in the conduction band, which form a metallic electron system. The reduced exciton masses obtained from the fits of the data shown in Fig. 5 are $0.068m_0$ and $0.064m_0$ in the $\text{Al}_x\text{Ga}_{1-x}\text{As}$ and $\text{In}_{1-x}\text{Ga}_x\text{As}_y\text{P}_{1-y}$ PQWs, respectively. The exciton heavy hole effective mass in GaAs, equal to $0.058m_0$, was calculated with the corresponding electron and heavy hole effective masses [29]. Using the data presented in Refs. [30–34], the reduced exciton masses expected in $\text{Al}_{0.24}\text{Ga}_{0.76}\text{As}$ and $\text{In}_{0.49}\text{Ga}_{0.51}\text{P}$ corresponding to the PQW boundaries are estimated as $0.075m_0$, and $0.078m_0$, respectively. Comparison of the experimentally obtained and calculated reduced masses of excitons indicates that the optical transitions observed in the PQWs studied here probably occur in the middle region of the PQW, which mainly consists of GaAs. In both PQWs, an effective Bohr radius of about 17 nm was obtained. In the next section, circular polarizations of PL radiation from confined levels will be determined in accordance with Eq. (1) and analyzed as functions of the magnetic field, taking into account the structure of the valence band, calculated both in $\text{Al}_x\text{Ga}_{1-x}\text{As}$ and $\text{In}_{1-x}\text{Ga}_x\text{As}_y\text{P}_{1-y}$ PQWs.

IV. RESULTS AND DISCUSSION

A multiband $\mathbf{k} \cdot \mathbf{p}$ formalism was developed based on the standard Kohn-Luttinger and parabolic Hamiltonian models to probe the electronic structure of holes and electrons, respectively. Exciton effects were not taken into account in the calculation, since the exciton binding energy determined in the previous Sec. III is considerably smaller than the changes in the energies of the confined levels of the valence band calculated as a function of the magnetic field. The electron and hole Hamiltonians are $\mathcal{H}_h = \mathcal{H}_{\text{KL}} + (V_{\perp}^h(z) + \mathcal{H}_z^h)I$ and $\mathcal{H}_e = \mathcal{H}_0 + (V_{\perp}^e(z) + \mathcal{H}_z^e)I$, where \mathcal{H}_{KL} is the 4×4 Kohn-Luttinger Hamiltonian, while $\mathcal{H}_0 = \hbar\omega_c a^{\dagger}a$ is spanned in the electron Bloch functions. $\mathcal{H}_z^h = -\hbar\omega_c(\kappa j_{hz} + q j_{hz}^3)$, where the cyclotron frequency $\omega_c = eB/m_0$ and $\mathcal{H}_z^e = -g_e\mu_B j_{ez}B$,

refer to hole and electron Zeeman energy terms, respectively. Here, q and κ are the magnetic Kohn-Luttinger parameters which define the g factor of holes, while g_e is the g factor of electrons and μ_B is the Bohr magneton. Finally, $V_{\perp}^{e(h)}(z)$ is the vertical confining potential for electrons (holes) and I is the identity matrix. The relevant y and z directions are shown in Fig. 1.

The influence of the magnetic field on the band structure was calculated similarly to the variational method described in detail in Ref. [35], using the zero field wavefunctions and energies of the valence band confined levels calculated in Sec. III. Then, solving the eigenvalue problem $(\mathcal{H}_h - E_v^h)\Psi_v^h = 0$, we get the eigenenergies E_v^h and eigenvectors $C_{n,s}^{j_z}$ of hole states:

$$\Psi_v^h = \sum_{n,s,j_z} C_{n,s}^{j_z} \Phi_n(y) h_s(z) |j_{hz}\rangle, \quad (4)$$

where n is the Landau level (LL) index and $\Phi_n(y)$ states the 1D harmonic oscillator motion in the y direction. The subband eigenfunctions h_s used in the $\mathbf{k} \cdot \mathbf{p}$ calculations were found by a self-consistent numerical solution of the system of Schrödinger-Poisson equations for the parabolic potential described in the previous section.

The Kohn-Luttinger band parameters (γ_i , q and κ) necessary for calculating the valence band structure in the $\text{Al}_x\text{Ga}_{1-x}\text{As}$ and $\text{In}_{1-x}\text{Ga}_x\text{As}_y\text{P}_{1-y}$ PQWs were obtained using linear interpolation between the parameters of the respective alloy components, taken from [34,36–41]. The Landau fan diagrams of the valence band thus obtained in the $\text{Al}_x\text{Ga}_{1-x}\text{As}$ and $\text{In}_{1-x}\text{Ga}_x\text{As}_y\text{P}_{1-y}$ PQWs are shown in Figs. 6(a) and 6(b) respectively, where, for the sake of clarity, only the relevant spin-polarized LLs of the heavy-hole $\text{HH}_{01}^{+/-}$, $\text{HH}_{03}^{+/-}$ and light-hole bands $\text{LH}_{01}^{+/-}$, where superscripts “+/-” refer to spin down/up, which make the largest contributions, are shown. The first and second subscripts indicate the numbers of the LL and the confined level, respectively. The hybridization between the heavy-hole and light-hole states causes a nonlinear dependence of the corresponding LL energies as a function of the magnetic field, resulting in the observable intersections between the states with different spins. Such intersections are the causes of the magnetic field-induced changes in the circular polarization P_{σ} emitted from corresponding confined levels shown in Fig. 6.

In the case of n-doped $\text{Al}_x\text{Ga}_{1-x}\text{As}$ and $\text{In}_{1-x}\text{Ga}_x\text{As}_y\text{P}_{1-y}$ PQWs, the Fermi-electron system is inert, while the PL circular polarization is determined by hole transitions between the levels of the valence band and is thus defined by the energy structures shown in Figs. 6(a) and 6(b). In this case, the hole polarization can be calculated according to the equation [42,43]:

$$P_h = \frac{\tanh\left(\frac{\Delta_s}{2kT}\right)}{1 + \zeta}, \quad (5)$$

where Δ_s is the valence band Zeeman splitting, $\zeta = \tau_s/\tau_0$ and the term $(1 + \zeta)^{-1}$ follows from a consideration of the spin relaxation dynamics in a system of two differently spin polarized states that decay to the ground state with the rate τ_0^{-1} , and there is a spin relaxation between the excited levels at a rate τ_s^{-1} . The condition $\tau_s < \tau_0$ ensures

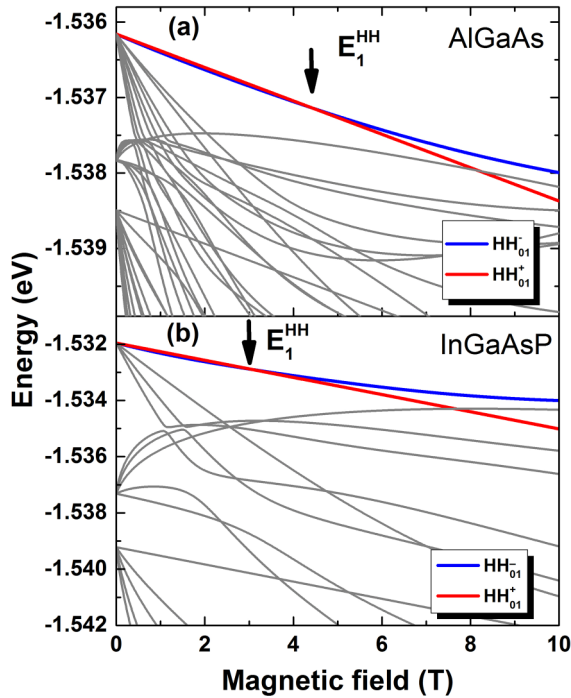


FIG. 6. The valence band LLs calculated in the $\text{Al}_x\text{Ga}_{1-x}\text{As}$ (a) and $\text{In}_{1-x}\text{Ga}_x\text{As}_y\text{P}_{1-y}$ (b) PQWs as a function of the magnetic field. The arrows indicate the intersections between LLs with different spin polarizations associated with the observed changes in the circular polarization of the corresponding confined levels caused by the magnetic field.

fast thermalization of holes into spin-polarized LL with the lowest energy and, consequently, different populations of spin-split LLs. The corresponding transitions are shown in Fig. 7. The spin polarizations of LLs were calculated using Eq. (5) with the magnetic field dependent Zeeman splittings Δ_s of the corresponding LLs shown in Fig. 6. The calculated LL polarizations were fitted to the related experimentally observed circular polarizations. As a consequence, the parameter ζ was obtained, which is subsequently used to determine the spin relaxation time τ_s .

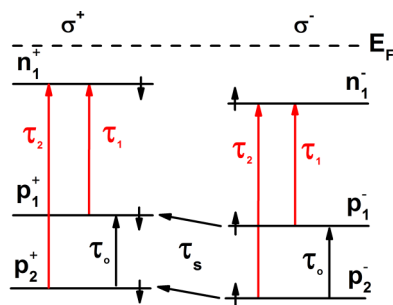


FIG. 7. Transfer processes of holes between LLs in $\text{Al}_x\text{Ga}_{1-x}\text{As}$ and $\text{In}_{1-x}\text{Ga}_x\text{As}_y\text{P}_{1-y}$ PQW. The solid red and black vertical arrows show the radiative interband and nonradiative intraband transitions, respectively. The interlevel energy relaxation time τ_0 and the spin relaxation time τ_s are responsible for the transfer between equally and differently spin polarized valence band LLs, respectively, while $\tau_{1(2)}$ is the corresponding interband recombination time.

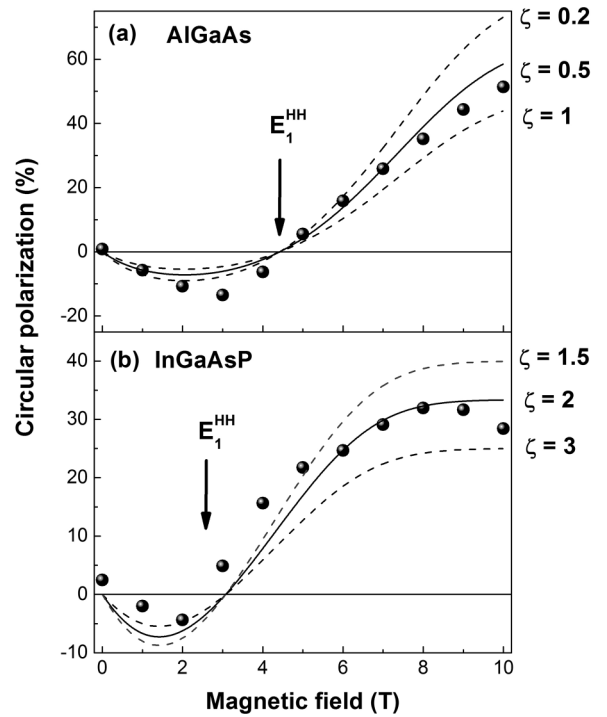


FIG. 8. Circular polarizations of the E_1^{HH} transitions measured in $\text{Al}_x\text{Ga}_{1-x}\text{As}$ (a) and $\text{In}_{1-x}\text{Ga}_x\text{As}_y\text{P}_{1-y}$ (b) PQWs as a function of the magnetic field. The corresponding polarizations of heavy hole LLs calculated by Eq. (5) with different parameters ζ are shown by solid and dashed lines. The arrows show the experimentally observed changes in the circular polarizations.

The circular polarizations of the optical transitions E_1^{HH} obtained according to Eq. (1) in the $\text{Al}_x\text{Ga}_{1-x}\text{As}$ PQW and the $\text{In}_{1-x}\text{Ga}_x\text{As}_y\text{P}_{1-y}$ PQW are shown in Fig. 8 as a function of the magnetic field. The low spectral definition of the E_1^{LH} and E_3^{HH} PL lines does not allow for determination of related polarizations. As noted above, the inversions of the optical polarization observed in both PQWs are due to the intersections between the corresponding valence band LLs with different spin polarizations. It is worth mentioning that the observed incomplete circular polarization of hole-confined levels is due to the effects of spin relaxation which are taken into account by the parameter ζ in Eq. (5). The best fits of the measured circular polarizations in the $\text{Al}_x\text{Ga}_{1-x}\text{As}$ and $\text{In}_{1-x}\text{Ga}_x\text{As}_y\text{P}_{1-y}$ PQWs were obtained with $\zeta = 0.5$ and 2, respectively. Thus, knowing the parameter ζ and the time of the interlevel transition τ_0 responsible for the energy relaxation of photogenerated holes, one can estimate the spin relaxation time of holes τ_s .

The interlevel transition time τ_0 was determined using the nonpolarized time-resolved PL measurements. In this case, the optical transition dynamics can be described by a simple three-level model, similar to that shown in Fig. 7, where interband transitions of photogenerated holes occur between two levels in the valence band with the corresponding populations p_1 and p_2 (spin is ignored) and a level in the conduction band at rates $1/\tau_1$ and $1/\tau_2$, respectively. For simplicity, optical transitions involving neutral carbon acceptors or DX centers, which can cause a long delay in PL, are not taken into account.

When limiting to only two levels in the valence band, which were clearly observed in both PQWs, the rate equations related to the radiative interband recombination have the form

$$\frac{dp_1}{dt} = -\frac{p_1}{\tau_1} + \frac{p_2}{\tau_0}, \quad (6)$$

$$\frac{dp_2}{dt} = -\frac{p_2}{\tau_2} - \frac{p_2}{\tau_0}. \quad (7)$$

The hole populations p_1 and p_2 are proportional to the intensities of the PL lines I_1 and I_2 , respectively, where I_1 and I_2 correspond to E_1^{HH} and E_3^{HH} transitions in the $\text{Al}_x\text{Ga}_{1-x}\text{As}$ PQW and E_1^{HH} and E_1^{LH} transitions in the $\text{In}_{1-x}\text{Ga}_x\text{As}_y\text{P}_{1-y}$ PQW. The solutions of the rate Eqs. (6) and (7) determine the time evolution of the populations of the considered levels of the valence band as

$$p_1(t) = C_1 e^{-\frac{t}{\tau_1}} - A e^{-\frac{t}{\tau^*}}, \quad (8)$$

$$p_2(t) = C_2 e^{-\frac{t}{\tau^*}}, \quad (9)$$

where $1/\tau^* = 1/\tau_0 + 1/\tau_2$, $A = C_2 \frac{\tau_1 \tau_2}{\tau_1 \tau_2 + \tau_0 \tau_1 - \tau_0 \tau_2}$, and C_1, C_2 are the constants. Finally, the interlevel transition time τ_0 can be expressed in terms of characteristic times and constants as follows:

$$\tau_0 = \frac{C_2}{A} \frac{\tau_1 \tau^*}{\tau_1 - \tau^*}. \quad (10)$$

Equations (8) and (9) were used to fit the experimental PL decay and thus, to determine the constants A and C_2 and the characteristic times τ_0 , τ_1 , and τ_2 .

The PL transients measured in the absence of a magnetic field in both PQWs at the energies of optical transitions attributed to the relevant confined levels are shown in Fig. 9, where the black dashed lines represent the best fits obtained by Eqs. (8) and (9). The small initial shoulder observed with increasing PL intensity is associated with the response of the detector used, which, at high pump power and short recombination time, can show two peaks in the instrument response function (IRF) due to its specific design. It should be noted that the solutions of Eqs. (8) and (9) contain the interlevel transition time τ_0 , which is responsible for the transfer of holes between the neighboring valence band confined levels. First, the high-energy confined level p_2 is filled. Then the filling of the low-energy confined level p_1 occurs during the time of the interlevel transition τ_0 from the confined level p_2 . This process causes a response delay which is experimentally observed as an initial increase in the PL intensity.

The PL transients measured in both PQWs reveal a weak long time delay, which is likely caused by neutral carbon acceptors or DX centers. As noted above, their contribution to the recombination dynamics was not considered, while monoexponential fast PL transients are attributed to radiative interband recombination and were fitted by Eqs. (8) and (9). The times τ_0 , τ_1 , and τ_2 obtained by best fits as a function of the magnetic field are shown in the insets to Figs. 9(a) and 9(b). In this case, the errors in determining the characteristic times do not exceed 2%.

As shown in the insets to Figs. 9(a) and 9(b), similar recombination times that are practically independent of the magnetic field were obtained in the $\text{Al}_x\text{Ga}_{1-x}\text{As}$ and $\text{In}_{1-x}\text{Ga}_x\text{As}_y\text{P}_{1-y}$ PQWs. Using the average interlevel

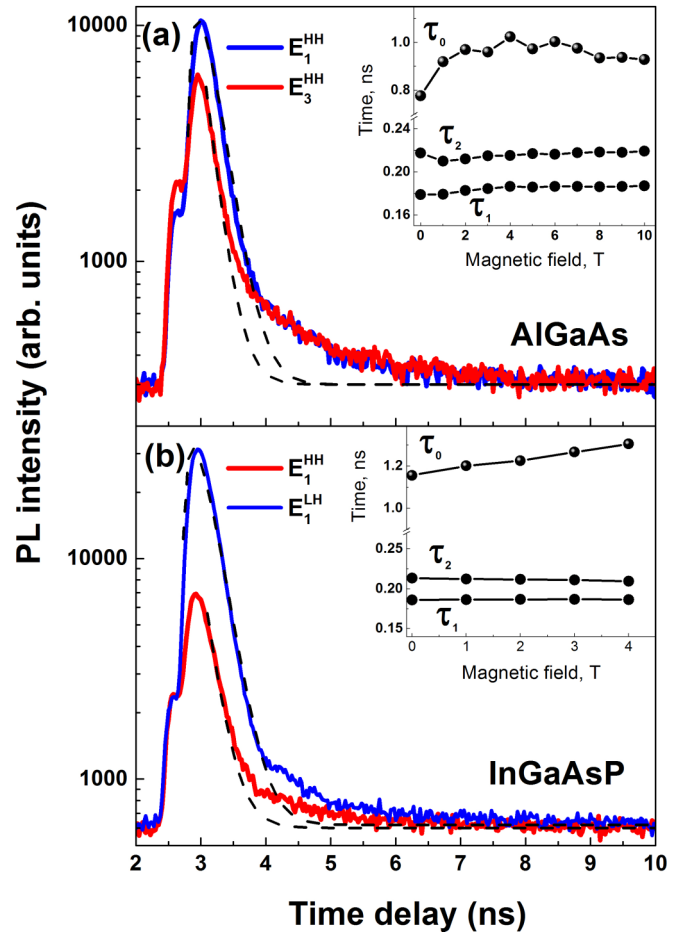


FIG. 9. PL transients measured without a magnetic field at $T = 1.6$ K in the $\text{Al}_x\text{Ga}_{1-x}\text{As}$ (a) and $\text{In}_{1-x}\text{Ga}_x\text{As}_y\text{P}_{1-y}$ (b) PQWs. The black dashed lines represent the best fits obtained by Eqs. (8) and (9). The insets show the corresponding recombination times as a function of the magnetic field.

transition times $\tau_0 = 0.95$ ns and 1.25 ns obtained in the $\text{Al}_x\text{Ga}_{1-x}\text{As}$ and $\text{In}_{1-x}\text{Ga}_x\text{As}_y\text{P}_{1-y}$ PQWs, respectively, and the related previously obtained parameters ζ , spin relaxation times of heavy holes were calculated: $\tau_s = 0.48$ ns and 2.5 ns in the $\text{Al}_x\text{Ga}_{1-x}\text{As}$ and $\text{In}_{1-x}\text{Ga}_x\text{As}_y\text{P}_{1-y}$ PQWs, respectively. Both these values are larger than the hole spin relaxation time of 30–60 ps reported in GaAs QWs [44–46]. In InGaAs/InP QWs an even shorter spin relaxation time as fast as 2–5 ps was measured [47,48]. However, the obtained long spin relaxation times are in good agreement with the spin relaxation time of about 1 ns obtained in similarly doped bulk GaAs [49]. This is consistent with the fact that PQW is considered as a quasi-three-dimensional structure. The spin relaxation times obtained in both studied PQWs, which are close to those of GaAs, are due to similar GaAs-like centers in both PQWs, in which recombination mainly occurs.

It is worth mentioning that the obtained heavy hole spin relaxation time is expected to be related to the Dyakonov-Perel interaction, which is the dominant mechanism of carrier spin relaxation in III–V semiconductors [50,51]. The Dyakonov-Perel mechanism regards the spin-flip processes as a result of the asymmetry of the constituent atoms in the zinc-blende

structure. The spin-orbit interaction in conjunction with the lack of inversion symmetry causes the spin splitting which acts as an effective magnetic field resulting in the spin-flip of carriers [52].

V. CONCLUSION

The optical properties of the quantum wells with parabolic potential composed of $\text{Al}_x\text{Ga}_{1-x}\text{As}$ and $\text{In}_{1-x}\text{Ga}_x\text{As}_y\text{P}_{1-y}$ alloys were studied. The parabolic shape of the potential energy results in accumulation of the photogenerated holes in the center of the PQWs, while the electrostatic repulsion among electrons forms a nearly square quantum well in the conduction band. As a consequence, the recombination between the photogenerated carriers takes place in the center region of the PQW. This causes two effects: (i) the center regions of both PQWs studied here are composed of GaAs; therefore, the spectral characteristics of both PQWs are found to be similar and (ii) holes mainly concentrated in the center of the PQW cause the radiation from even confined states to disappear. Thus, the discussed effect of the disappearance of radiation from even confined states is the result of the specific structure

of the conduction band and the valence band, which leads to a different spatial distribution of electrons in the conduction band and photogenerated holes in the valence band. Moreover, at a certain magnetic field the hybridization between the heavy-hole and light-hole states results in intersections between the LLs with different spins which was found to be responsible for the observed change in the PL circular polarization. Fitting the calculated circular polarization to the measured one, together with time-resolved PL analysis, made it possible to estimate the characteristic spin relaxation time of holes in both PQWs under study. The resulting spin relaxation time turned out to be much longer than expected in GaAs QWs, but close to bulk GaAs.

ACKNOWLEDGMENTS

Brazilian agencies FAPESP (Grant No. 2022/02132-0), CNPq (Grant No. 301013/2019-5), CAPES (Grant PNPd 88887.336083/2019-00), and the Natural Sciences and Engineering Research Council of Canada (Grant No. RGPIN-2018-04015) are gratefully acknowledged.

-
- [1] R. C. Miller, A. C. Gossard, D. A. Kleinman, and O. Munteanu, *Phys. Rev. B* **29**, 3740 (1984).
- [2] B. I. Halperin, *Jpn. J. Appl. Phys.* **26**, 1913 (1987).
- [3] K.-X. Guo and S.-W. Gu, *Phys. Rev. B* **47**, 16322 (1993).
- [4] R. Bratschitsch, T. Müller, R. Kersting, G. Strasser, and K. Unterrainer, *Appl. Phys. Lett.* **76**, 3501 (2000).
- [5] K. D. Maranowski, A. C. Gossard, K. Unterrainer, and E. Gornik, *Appl. Phys. Lett.* **69**, 3522 (1996).
- [6] G. Wang, *Phys. Rev. B* **72**, 155329 (2005).
- [7] M. Geiser, F. Castellano, G. Scalari, M. Beck, L. Nevou, and J. Faist, *Phys. Rev. Lett.* **108**, 106402 (2012).
- [8] T. Chakraborty and P. Pietiläinen, *Phys. Rev. Lett.* **95**, 136603 (2005).
- [9] A. L. Efros and E. I. Rashba, *Phys. Rev. B* **73**, 165325 (2006).
- [10] M. Studer, G. Salis, K. Ensslin, D. C. Driscoll, and A. C. Gossard, *Phys. Rev. Lett.* **103**, 027201 (2009).
- [11] M. W. Wu, J. H. Jiang, and M. Q. Weng, *Phys. Rep.* **493**, 61 (2010).
- [12] W. Kohn, *Phys. Rev.* **123**, 1242 (1961).
- [13] L. Brey, N. F. Johnson, and B. I. Halperin, *Phys. Rev. B* **40**, 10647 (1989).
- [14] R. F. Kopf, M. H. Herman, M. Lamont Schnoes, A. P. Perley, G. Livescu, and M. Ohring, *J. Appl. Phys.* **71**, 5004 (1992).
- [15] A. Ballabio, J. Frigerio, S. Firoozabadi, D. Christina, A. Beyer, K. Volz, and G. Isella, *J. Phys. D: Appl. Phys.* **52**, 415105 (2019).
- [16] S. Sen, F. Capasso, A. C. Gossard, and R. A. Spah, *Appl. Phys. Lett.* **51**, 1428 (1987).
- [17] A. M. Ortiz de Zavallos, N. C. Mamani, G. M. Gusev, A. A. Quivy, T. E. Lamas, and J. C. Portal, *Phys. Rev. B* **75**, 205324 (2007).
- [18] Y. Ohno, D. K. Young, B. Beschoten, F. Matsukara, H. Ohno, and D. D. Awschalom, *Nature (London)* **402**, 790 (1999).
- [19] N. V. Baidus, M. I. Vasilevskiy, M. J. M. Gomes, M. V. Dorokhin, P. B. Demina, E. A. Uskova, B. N. Zvonkov, V. D. Kulakovskii, A. S. Brichkin, A. V. Chernenko, and S. V. Zaitsev, *Appl. Phys. Lett.* **89**, 181118 (2006).
- [20] B. Huang, X. K. Cao, H. X. Jiang, J. Y. Lin, and S.-H. Wei, *Phys. Rev. B* **86**, 155202 (2012).
- [21] I.-H. Tan, G. L. Snider, and E. L. Hu, *J. Appl. Phys.* **68**, 4071 (1990).
- [22] L. Pavesi and M. Guzzi, *J. Appl. Phys.* **75**, 4779 (1994).
- [23] K. M. S. V. Bandara, D. D. Coon, Byung-sung O, Y. F. Lin, and M. H. Francombe, *Appl. Phys. Lett.* **53**, 1931 (1988).
- [24] P. Christol, P. Lefebvre, and H. Mathieu, *J. Appl. Phys.* **74**, 5626 (1993).
- [25] S. N. Walck and T. L. Reinecke, *Phys. Rev. B* **57**, 9088 (1998).
- [26] M. Hayne, R. Provoost, M. K. Zundel, Y. M. Manz, K. Eberl, and V. V. Moshchalkov, *Phys. Rev. B* **62**, 10324 (2000).
- [27] D. C. Rogers, J. Singleton, R. J. Nicholas, C. T. Foxon, and K. Woodbridge, *Phys. Rev. B* **34**, 4002 (1986).
- [28] M. Hayne, J. Maes, S. Bersier, M. Henini, L. Müller-Kirsch, R. Heitz, D. Bimberg, and V. V. Moshchalkov, *Phys. B: Condens. Matter* **346-347**, 421 (2004).
- [29] J. Singh, *Physics of Semiconductors and Their Heterostructures* (McGraw-Hill, 1993).
- [30] P. Wolf, *IBM J. Res. Dev.* **14**, 125 (1970).
- [31] G. D. Vendelin, *Design of Amplifiers and Oscillators by the S-Parameter Method* (Wiley, 1982).
- [32] *Properties of Aluminium Gallium Arsenide*, edited by S. Adachi, EMIS Datareviews Series No. 7 (INSPEC, The Institute of Electrical Engineers, London, UK, 1993).
- [33] *Properties of Lattice-Matched and Strained Indium Gallium Arsenide*, edited by P. Bhattachary, EMIS Datareviews Series No. 8 (INSPEC, Institute of Engineers & Technology, London, UK, 1993).
- [34] I. Vurgaftman, J. R. Meyer, and L. R. Ram-Mohan, *J. Appl. Phys.* **89**, 5815 (2001).

- [35] L. F. dos Santos, Yu. A. Pusep, L. Villegas-Lelovsky, V. Lopez-Richard, G. E. Marques, G. M. Gusev, D. Smirnov, and A. K. Bakarov, *Phys. Rev. B* **86**, 125415 (2012).
- [36] B. V. Shanabrook, O. J. Glembocki, D. A. Broido, and W. I. Wang, *Phys. Rev. B* **39**, 3411(R) (1989).
- [37] J.-H. Park, L. H. Tjeng, J. W. Allen, P. Metcalf, and C. T. Chen, *Phys. Rev. B* **55**, 12813 (1997).
- [38] L. Vervoort, R. Ferreira, and P. Voisin, *Semicond. Sci. Technol.* **14**, 227 (1999).
- [39] S. Richard, F. Aniel, and G. Fishman, *Phys. Rev. B* **70**, 235204 (2004).
- [40] O. Drachenko, D. V. Kozlov, V. Ya. Aleshkin, V. I. Gavrilenko, K. V. Maremyanin, A. V. Ikonnikov, B. N. Zvonkov, M. Goiran, J. Leotin, G. Fasching, S. Winnerl, H. Schneider, J. Wosnitza, and M. Helm, *Phys. Rev. B* **79**, 073301 (2009).
- [41] G. Linares García and L. Meza-Montes, *Rev. Mex. Fís.* **65**, 231 (2019).
- [42] M. I. Dyakonov and V. I. Perel, in *Optical Orientation*, edited by F. Meier and B. P. Zakharchenya (Elsevier, Amsterdam, 1984).
- [43] B. Kovalski, P. Omling, B. K. Meyer, D. M. Hofmann, V. Härle, F. Scholz, and P. Sobkowicz, *Semicond. Sci. Technol.* **11**, 1416 (1996).
- [44] S. D. Ganichev, S. N. Danilov, V. V. Bel'kov, E. L. Ivchenko, M. Bichler, W. Wegscheider, D. Weiss, and W. Prettl, *Phys. Rev. Lett.* **88**, 057401 (2002).
- [45] M. Syperek, D. R. Yakovlev, A. Grelich, J. Misiewicz, M. Bayer, D. Reuter, and A. D. Wieck, *Phys. Rev. Lett.* **99**, 187401 (2007).
- [46] T. Ostatnický, O. Crégut, M. Gallart, P. Gilliot, B. Hönerlage, and J.-P. Likforman, *Phys. Rev. B* **75**, 165311 (2007).
- [47] A. Tackeuchi, O. Wada, and Y. Nishikawa, *Appl. Phys. Lett.* **70**, 1131 (1997).
- [48] M. A. Tito Patricio, M. D. Teodoro, G. M. Jacobsen, R. R. LaPierre, and Yu. A. Pusep, *Phys. E: Low-dimens. Syst. Nanostruct.* **143**, 115347 (2022).
- [49] R. I. Dzhioev, K. V. Kavokin, V. L. Korenev, M. V. Lazarev, B. Ya. Meltser, M. N. Stepanova, B. P. Zakharchenya, D. Gammon, and D. S. Katzer, *Phys. Rev. B* **66**, 245204 (2002).
- [50] A. Tackeuchi, Y. Nishikawa, and O. Wada, *Appl. Phys. Lett.* **68**, 797 (1996).
- [51] S. Fang, R. Zhu, and T. Lai, *Sci. Rep.* **7**, 287 (2017).
- [52] M. I. Dyakonov and V. I. Perel, *Z. Eksp. Teor. Fiz.* **60**, 1954 (1971) [*Sov. Phys. JETP* **33**, 1053 (1971)].